ACS APPLIED MATERIALS & INTERFACES

Research Article

Cite This: ACS Appl. Mater. Interfaces 2018, 10, 27795−27800

www.acsami.org

Conductive Binder for Si Anode with Boosted Charge Transfer Capability via n-Type Doping

Yan Zhao,[†,#] Luyi Yang,[†,#] Yunxing Zuo,[‡] Zhibo Song,[§] Fang Liu,[†] Ke Li,[†] and Feng Pan*[,†]

[†]School of Advanced Materials, Peking University Shenzhen Graduate School, Shenzhen 518055, P. R. China

[‡]Department of Nano Engineering, University of California San Diego, 9500 Gilman Drive 0448, La Jolla, California 92093-0448, United States

[§]School of Materials Science and Engineering, Zhengzhou University, Zhengzhou 450001, P. R. China

Supporting Information

ABSTRACT: Employing conductive binders in silicon (Si) anode has been considered as a fundamental solution to the pulverization of Si particles. Therefore, it is still a great challenge to improve the charge transfer capability of the conductive binder. Herein, a copolymer (PFPQ-COONa) is synthesized, characterized, and electrochemically tested as conductive binder for Si anode. It is found that PFPQ-COONa exhibits not only excellent cycling stability, but also satisfactory rate performance with relatively high areal loading, which outperforms currently reported single-component conductive binders. The superior electrochemical performance can be attributed to the molecular-level contact between binder and Si particles and to the enhanced intrinsic conductivity of PFPQ-COONa at reductive potential. This method provides a fresh perspective to design and develop conductive binder for high-capacity battery anode.

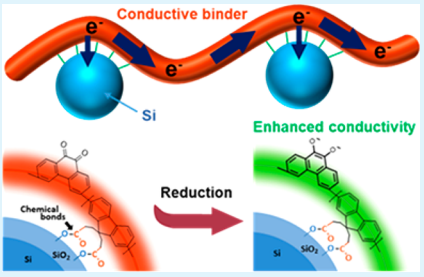

KEYWORDS: *Li-ion battery, Si anode, conductive binder, n-type doping, rate capability*

INTRODUCTION

Lithium ion batteries (LIBs) with higher energy density are desirable for the development of electronic vehicles (EVs).[1,2] The relatively low theoretical capacity (372 mA h g^{-1}) of commercial graphite anode greatly limits the application of LIBs in EVs. Hence, it is critical to develop alternative anode materials with high theoretical capacities. Silicon (Si) anode has attracted wide attention due to its abundance and appealing theoretical capacity (4200 mA h g^{-1}). However, unlike insertion anode materials, the fully lithiated phase of Si anode ($Li_{15}Si_4$) suffers from drastic volume change[3] (approximately 300%), which can cause pulverization of active materials and unstable solid-electrolyte interphase (SEI), eventually leading to capacity decay.[4]

In recent years, extensive efforts have been made to improve the cycling stability of Si anode. Various methods such as using nanosized Si,[5,6] controlling operating voltages,[3] and combining Si with carbon materials (e.g., graphite,[7] carbon nanotubes,[8] graphene,[9] and amorphous carbon[10]) have been employed for the purpose of alleviating the volume expansion effects. As an important component in Si anode, different types of binders have also been investigated.[11] Conventional binders such as polyvinylidene difluoride (PVDF),[12] sodium carboxymethyl cellulose (CMC-Na),[13] poly(acrylic acid) (PAA),[12,14] and polysaccharides[15,16] have been widely tested as binder for Si anode. However, these binders cannot inherently prevent the capacity fading caused by pulverization of Si particles—once Si particles lose contact with conductive materials during the cycling process, they become electronically inactive.

To provide a fundamental solution for Si anode, conductive binders have been proposed to replace conventional binders. Polyaniline,[17,18] poly(3,4-ethylenedioxythiophene) polystyrenesulfonate (PEDOT:PSS),[19−21] guar gum,[22] and polyfluorenes[23−25] have been studied as conductive binders in Si anode. Most works above have focused on synthesizing or employing binders with high electric conductivity. However, the rate of charge transfers between the binder and Si during charge−discharge of LIBs depends on two factors: the charge transfers within the binder and the rate of interfacial charge transfers between the binder and the active particle (e.g., Si), respectively. Therefore, unlike conventional binders, it is necessary for conductive binder to have good conductivity in addition to enhanced interfacial charge transfers by maintaining close contact with active materials. In our previous work, it was found that as a conductive binder, sodium poly(9,9-bis(3-propanoate) fluorene) (PF-COONa) could effectively enhance the cycling stability of Si anodes by exhibiting good adhesive property, high electrolyte uptake, and electric conductivity. More importantly, the binder managed to maintain electronic integrity of the electrode despite huge volume changes, which leads to good cycling stability.[26] It has also been reported that

Received: May 31, 2018
Accepted: July 30, 2018
Published: July 30, 2018

DOI: 10.1021/acsami.8b08843
ACS Appl. Mater. Interfaces 2018, 10, 27795−27800

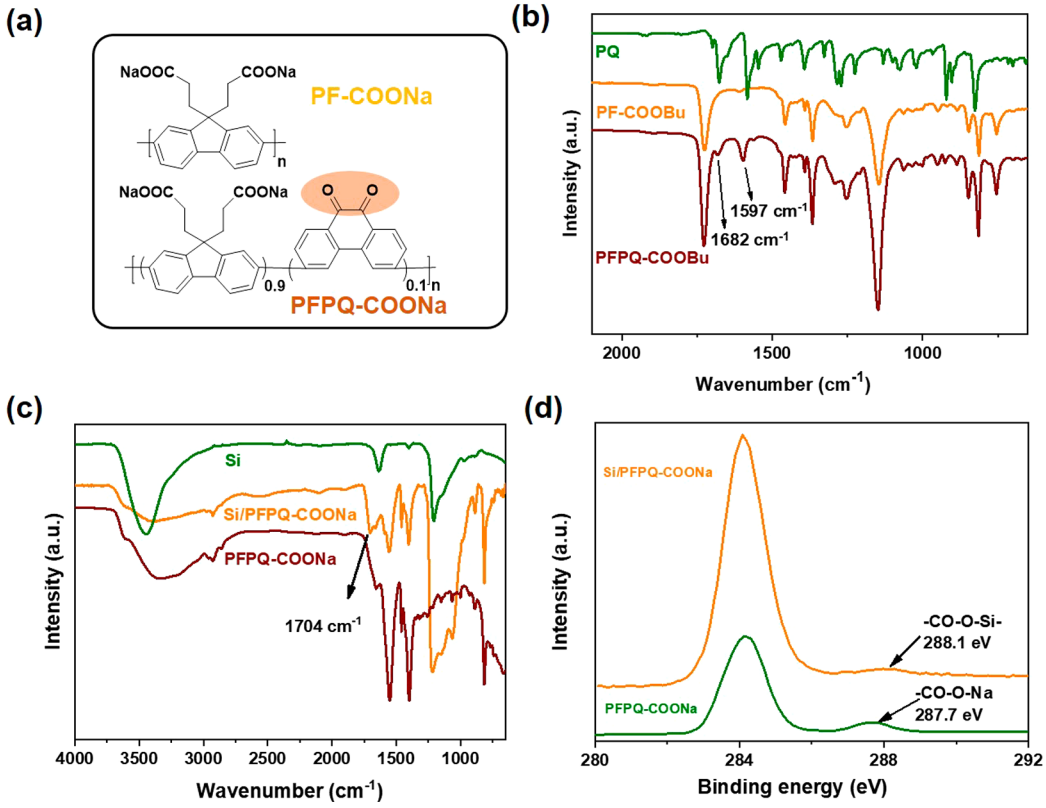

Figure 1. (a) Proposed molecular structure of PF-COONa and PFPQ-COONa; (b) FTIR spectra of PQ, PF-COOBu, and PFPQ-COOBu; (c) FTIR spectra of Si particles, Si/PFPQ-COONa, and PFPQ-COONa; (d) XPS results of Si/PFPQ-COONa and PFPQ-COONa.

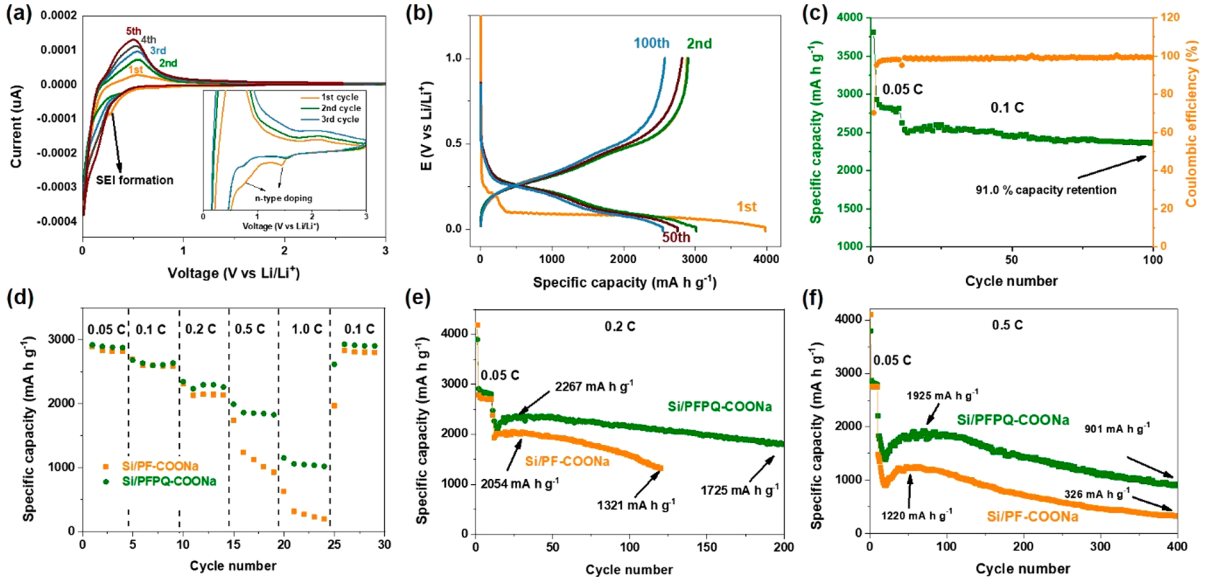

Figure 2. (a) Cyclic voltammogram of Si/PFPQ-COONa electrode for different cycle numbers; (b) voltage profiles of Si/PFPQ-COONa for different cycle numbers at 0.05 C; (c) cycling performance of Si/PFPQ-COONa at 0.1 C; (d) rate performances of Si/PF-COONa and Si/PFPQ-COONa; (e) cycling performance of Si/PF-COONa and Si/PFPQ-COONa at 0.2 C; (f) cycling performance of Si/PF-COONa and Si/PFPQ-COONa at 0.5 C. For all measurements above, the areal loading of the active material was approximately 1.2 mg cm^{-2}.

poly(phenanthraquinone) (PPQ) shows excellent rate capability as a conductive binder for Si anode.[27] However, long-term cycling performance of PPQ/Si is not provided and the mechanism behind its good electrochemical performance remains unclear. To combine advantages of the excellent rate capability of PPQ and the good cycling stability of PF-COONa, herein, a novel copolymer (PFPQ-COONa) is prepared and tested as binder for Si anode by introducing 10% of phenanthraquinone (PQ) into PF-COONa.

RESULTS AND DISCUSSION

As shown in Figure 1a, the as-prepared PFPQ-COONa (M_n = 11 428, M_w/M_n = 2.49) contains 10 mol % of PQ group in the backbone of PF-COONa. To confirm whether the desired

DOI: 10.1021/acsami.8b08843
ACS Appl. Mater. Interfaces 2018, 10, 27795−27800

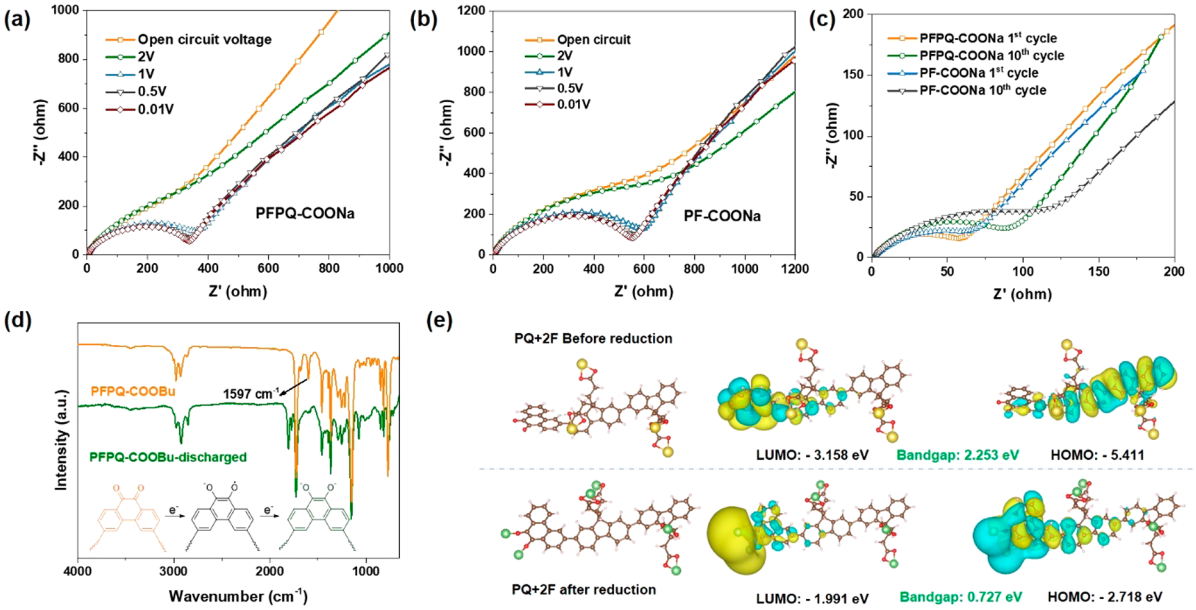

Figure 3. Electrochemical impedance spectra of (a) PFPQ-COONa and (b) PF-COONa polymer pellet in the presence of electrolyte under different potential vs Li/Li^+ (diameter and thickness of the polymer pellet are approximately 12 mm and 0.025 mm, respectively); (c) electrochemical impedance spectra of half cells using different binders after the first and the 10th cycle; (d) proposed reduction reaction of PQ and FTIR spectra of PFPQ-COOBu before and after discharging; (e) molecular structures and molecular frontier orbitals of initial state and reduced state of PQ+2F segments.

copolymer was obtained, Fourier transform infrared (FTIR) spectroscopy was used to characterize the products. Figure 1b presents the FTIR spectra of the products before acid-hydrolyzation (PF-COOBu and PFPQ-COOBu). It can be seen that the spectra of PF-COOBu and PFPQ-COOBu are very similar except that PFPQ-COOBu shows extra peaks at 1597 and 1682 cm^{-1}, which refer to the stretching vibrations for carbonyl group. According to the ^1H NMR spectrum, it was found that the surface integral ratio of different H elements in the ^1H NMR spectrum is about 4:4.17:6.77, which is very close to the theoretical value of PFPQ-COONa (4:4:6.67). The mechanical properties of PFPQ-COONa have also been tested. The hardness and the Young's modulus of the polymer film were measured to be 0.14 and 5.48 GPa, respectively. The swelling test was also performed in order to estimate the electrolyte uptake of PFPQ-COONa. From Supporting Information Figure S1 it can be seen that PFPQ-COONa exhibits higher electrolyte uptake compared with PF-COONa. The prepared Si anode consists of 70 wt % of nanosized Si (with diameter of 60 nm) and 30 wt % of PFPQ-COONa. Furthermore, after the electrode preparation, the FTIR spectra of PFPQ-COONa, Si, and Si/PFPQ-COONa are compared in Figure 1c. It can be clearly observed that compared to pristine PFPQ-COONa, two characteristic bands at 1560 cm^{-1} (asymmetric stretching vibration) and 1407 cm^{-1} (symmetric stretching vibration) for carboxylic acid salt[28] are weakened while a new peak at 1704 cm^{-1} (stretching vibration of carbonyl group) is formed, indicating new O═C—OR groups are resulted from the O═C—ONa groups.[29] This result strongly indicates that PFPQ-COONa can form chemical bond (O═C—OSi) with the SiO_2 on Si surface. In addition, from the C 1s X-ray photoelectron spectra (XPS) in Figure 1d, the formation of O═C—OR group from —COONa can also be observed since the bonding energy of —COONa of PFPQ-COONa shifts from 287.7 to 288.1 eV when it is prepared into anode with Si, which agrees with the FTIR results and further confirms that chemical bonds are formed between the conductive binder and Si particles. To test the chemical stability of PFPQ-COONa, the electrode with PFPQ-COONa binder was immersed into the electrolyte for 48 h. From the FTIR spectrum (Figure S2) it can be seen that the electrolyte-treated electrode shows almost unchanged absorbance spectrum, suggesting good electrolyte stability. The electrochemical stability of PFPQ-COONa was examined with linear sweep voltammogram (LSV). As shown in Figure S3, the decomposition voltage of PFPQ-COONa is approximately 3.69 V, which meets the demands for all types of anode material.

Figure 2a demonstrates the cyclic voltammogram (CV) of Si/PFPQ-COONa anode at the sweep rate of 0.1 mV s^{-1}. It can be seen that the onset potential for Li—Si alloying is around 0.67 V while a broad anodic band is found between 0.25 and 0.55 V, showing the dealloying process. The increasing current density with cycle number refers to the gradual activation process of Si anode. From the curve of first cycle it can be seen that during the cathodic sweeping, two reduction peaks are obtained around 0.75 and 1.5 V (Figure 2a, inset). As previously stated, these reactions can be ascribed to the n-type doping process of PF-COONa backbone,[26] which contributes to its conductivity. In addition, the peak at 0.28 V is caused by the formation of solid electrolyte interface (SEI) layer on the surface of anode. Figure 2b shows the voltage profiles of Si/PFPQ-COONa electrode at the C-rate of 0.05 C. The first discharge curve shows a long plateau at 0.08 V with a capacity of 3982 mA h g^{-1}, denoting the alloying of crystalline Si. During the second cycle a reversible capacity of 3015 mA h g^{-1} is obtained at the second cycle, which shows a characteristic discharge profile referring to the alloying of amorphous Si, and it is also observed that after 100 cycles the charge/discharge curves remain almost unchanged. The cycling performance of Si/PFPQ-COONa at 0.1 C is presented in Figure 2c, where the C-rate of 0.05 C is applied

DOI: 10.1021/acsami.8b08843
ACS Appl. Mater. Interfaces 2018, 10, 27795−27800

for the first 10 cycles until a stable capacity is reached. It can be seen that the Coulombic efficiencies are retained over 98% for over 100 cycles and 91.0% of reversible capacity can be obtained, indicating excellent cycling stability. To determine whether incorporating PQ into PF-COONa can boost the electrochemical performances of Si anode, the rate capability and cycling stability of Si anodes using PF-COONa and PFPQ-COONa are compared in Figure 2d. It can be seen that at lower C-rates (0.05 and 0.1 C), the two cells show very similar capacities. Si/PFPQ-COONa starts to deliver distinctly higher capacities when the C-rate is beyond 0.2 C. When the C-rate reaches 0.5 and 1 C, the average capacities for Si/PFPQ-COONa are 1850 mA h g^{-1} (0.5 C) and 1051 mA h g^{-1} (1 C) while the values for Si/PF-COONa are only 1214 mA h g^{-1} (0.5 C) and 330 mA h g^{-1} (1 C). As the C-rate is reverted back to 0.1 C, capacities for both cells can be well recovered, but the average capacity for Si/PFPQ- COONa is still slightly higher than that of Si/PF-COONa. These results have revealed that PFPQ-COONa exhibits significantly improved rate capability without compromising the excellent cycling stability of PF-COONa. Results from long-term cycling tests also agree with this conclusion. From Figure 2e, it can be observed that although at 0.2 C, the two cells delivered similar initial capacities. However, as cycling continues, Si/PFPQ-COONa shows a much better capacity retention (76.1% after 200 cycles) compared to that of Si/PF-COONa (64.3% after 120 cycles). In addition, the initial Coulombic efficiency of Si/PFPQ-COONa is also higher than that of Si/PF-COONa. By combining this result with the rate performances, it can be speculated that with this active material loading, the good cycling stability of PF-COONa cannot be retained at 0.2 C while PFPQ-COONa still manages to deliver good cycling stability. As expected, the discrepancy is even larger as the rate increases to 0.5 C. As shown in Figure 2f, the highest capacity obtained from Si/PFPQ-COONa (1925 mA h g^{-1}) is much higher than that of Si/PF-COONa (1220 mA h g^{-1}). After 400 cycles, a specific capacity of 901 mA h g^{-1} is obtained for Si/PFPQ-COONa, corresponding to a capacity retention of 46.8%, which also outperforms Si/PF-COONa (326 mA h g^{-1}, with 26.7% retention). In this case, the good cycling stability is ascribed to the PFPQ-COONa backbone and the enhanced rate performance is due to the added PQ group, which will be discussed later.

Electrochemical impedance spectroscopy (EIS) measurements were performed to understand the origin of better rate capability for Si/PFPQ-COONa. The impedance spectra of both binders at different potential vs Li/Li^+ are presented in Figure 3a and 3b. It can be seen that at open circuit voltage (OCV), both cells exhibit very similar resistances. By negatively scanning the potential from 2 to 1 V, the charge-transfer impedance (R_{ct}) of both binders sharply decreases, which can be attributed to the n-type doping that occurs at 1.5 V (see Figure 3a). As the potential reaches 0.5 V, the R_{ct} of both polymers further decreases, corresponding to the n-type doping at 0.75 V (also see Figure 3a). The impedances remain almost unchanged when the potential is swept to 0.01 V, indicating no further n-type doping within this voltage range. From the impedance, the conductivity of PFPQ-COONa after doping is much higher than that of the PF-COONa. Furthermore, by comparing the impedances of half cells after cycling (shown in Figure 3c), it can also be observed that the cell using PFPQ-COONa exhibits lower R_{ct} than that of the cell using PF-COONa, suggesting the superior conductivity of PF-COONa can be retained after cycling. Therefore, the improved conductivity of PFPQ-COONa should explain its better rate performance. It has been previously reported that the two carbonyl groups in PQ can be electrochemically reduced to −O− groups stepwise.[30,31] Although the measured direct current (DC) conductivity of bare PFPQ-COONa is relatively low (1.4×10^{-6} S cm^{-1}), it can be greatly improved after n-type doping reaction. Herein, in order to confirm this reaction in the polymer, PFPQ-COOBu was electrochemically reduced. Then the reduced PFPQ-COOBu was examined and compared with pristine PFPQ-COOBu via FTIR spectroscopy. As shown in Figure 3d, after discharge, the peak at 1597 cm^{-1} corresponding to the stretching vibration of carbonyl group has significantly diminished, which confirms the reduction of carbonyl group. Consequently, it can be also considered that the formed −O− groups will form −O−Li groups with Li-ions. To have an in-depth knowledge of the intrinsic relationship between the improved conductivity and the structure of PFPQ-COOBu, computational simulations have been performed. In this case, a segment consisting of one PQ and two fluorene molecules is studied for simplicity. Figure 3e shows the calculated highest-occupied molecular orbital (HOMO) and lowest-unoccupied molecular orbital (LUMO) molecular orbitals distribution for both initial state and reduced state of the segment. Note that sodium ions in the polymer can be readily substituted with lithium ions in the electrolyte. After the double bond of carbonyl being reduced, leaving negatively charged oxygen ions simultaneously bonded with dissociative lithium ions, ultimately forming a charge balanced system. The comparison of molecular orbital distribution between initial state and reduced state of the segment strongly indicates increased chemical activity located in the reduced PQ group. The donor units had been transferred to the reduced carbonyl during rapid reduction process, introducing high electrochemical reactivity in reduced carbonyl group. More importantly, the band gap decreases from 2.253 to 0.727 eV after the reduction process, resulting in enhanced electron conductivity. This qualitative result in good accordance with the results shown in Figure 3a and 3b where the conductivity of PFPQ-COONa is similar to that of PF-COONa at OCV, then the discrepancy starts to show at lower voltage. Therefore, one can assume that at low voltage, PQ undergoes a 2-electron reduction (i.e., n-type doping), which is much stronger than the n-type doping of PF-COONa and further leads to improved conductivity.

CONCLUSIONS

To conclude, a new conductive polymer binder for Si anode (PFPQ-COONa) was prepared by introducing 10% of PQ into PF-COONa. Galvanostatic cycling results demonstrate that PFPQ-COONa exhibits not only excellent cycling stability, but also significantly improved rate capability compared to PF-COONa. The superior electrochemical performance of PFPQ-COONa outperforms most currently reported conductive binders (see Table S1). Note that PFPQ-COONa is a single-component binder, which can be blended with other polymers in order to further improve its conductivity or adhesion ability. The electrochemical performances of PFPQ-COONa can be attributed to its well-designed molecular structure (as illustrated in Scheme 1). On the one hand, the formed −COOSi− groups between PFPQ-COONa and Si particle act as anchoring point, which facilitates a molecular level of contact between the conductive network and Si particles

DOI: 10.1021/acsami.8b08843
ACS Appl. Mater. Interfaces 2018, 10, 27795−27800

Scheme 1. Schematic Illustration of the Electrochemical Behavior of PFPQ-COONa Binder in Si Anode

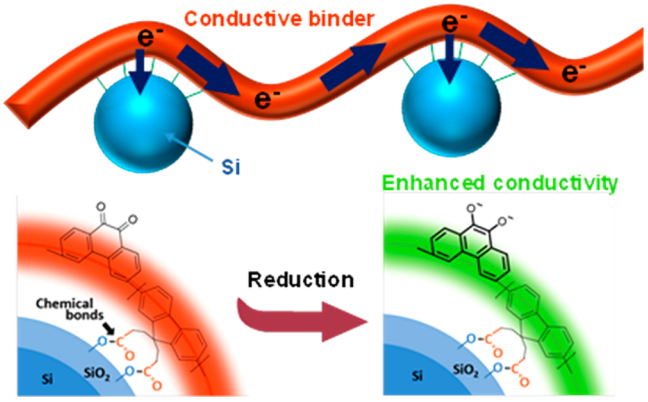

during the lithium alloying and dealloying. As a result, the average distance between Si particles and polymer chains is greatly shortened, which benefits the charge transfers at the interface. On the other hand, the carbonyl groups in PQ can be reduced into −O−Li groups at reductive potential, greatly boosting the conductivity of the binder, hence the improved rate performance. In addition to its conductivity, the good mechanical property of PFPQ-COONa also contributes to its excellent cycling stability. This approach provides a new perspective on rational designing of high-performance conductive binder for Si anode: good interfacial charge transfers are equally important as high intrinsic conductivity of the conductive binder, which can be smartly tuned by introducing functional groups with desirable properties.

EXPERIMENTAL METHODS

The materials for synthesis of polymers were purchased from TCI or sigma and the used tetrahydrofuran (THF) was distilled in the presence of Na with benzophenone. The compounds M1 and M2 and the polymer PF-COONa (shown in Figure S1) were synthesized according to the literature.[26]

Synthesis of PFPQ-COOBu. A mixture of 2,7-dibromo-9,9-bis(3-(*tert*-butyl propanoate))fluorene (M1) (0.9286 g, 1.6 mmol), 2-(4,4,5,5-tetramethyl-1,3,2-dioxaborolan-2-yl)-9,9-bis(3-(*tert*-butyl propanoate))fluorene (M2) (1.3490 g, 2.0 mmol), 3,6-dibromo-phenanthrenequinone (M3) (0.1464g, 0.4 mmol), (PPh3)4Pd(0) (0.046 g, 0.04 mmol), and several drops of Aliquat 336 were placed in a pressure tube. Fifteen mL of distilled THF and 5 mL of 2 M Na_2CO_3 were added at Ar atmosphere and then the mixture was stirred vigorously at 85 °C for 3 d. After the reaction stopped, the solution was poured into methanol and the polymer was obtained by vacuum filtration. The resulting polymer was washed by deionized water and further purified by precipitating from methanol twice. The precipitated solid was collected by vacuum filtration and dried under vacuum. The orange−red product was obtained with a yield of 90%. ^{1}H NMR (TMS, $CDCl_3$), δ(ppm): 7.88 (m, Ar−H), 7.73 (m, Ar−H), 7.64 (m, Ar−H), 2.55 (br s, CH_2), 1.65 (br s, CH_2), 1.31 (s, CH_3).

Synthesis of PFPQ-COONa. PFPQ-COOBu (1 g) was dissolved in dichloromethane solution with 15 wt % trifluoroacetic acid (50 mL). The mixture was stirred overnight at room temperature. After the reaction completed, the solvent was removed and the dark red residue was treated with aqueous Na_2CO_3 (0.1 M, 50 mL) at room temperature for 10 h. The polymer was purified by dialysis against deionized water for 5 days. The solution was then freeze-dried to give PFPQ-COONa (yield, 95%) as a dark red solid. ^{1}H NMR (400 M Hz, $CDCl_3$), δ(ppm): 7.84−7.93 (m, Ar−H); 2.48 (br s, CH_2); 1.48 (br s, CH_2).

Material Characterizations. FTIR spectra were collected on a Nicolet Avatar 360 spectrophotometer (KBr tablet). Nuclear magnetic resonance (NMR) spectrometry (^{1}H NMR and ^{13}C NMR) was recorded on a Bruker DPX 400 MHz spectrometer. XPS data of samples were collected with ESCALAB 250Xi. TGA was carried out with a Seiko Exstar 6000 instrument at a scanning rate of 10 °C min^{-1} in nitrogen atmosphere. The hardness and Young's Modulus were measured on an Agilent G200 Nano Indenter. The molecular weight was measured on a Viscotek TDA305 gel permeation chromatograph (Malvern). The swelling test was carried out by pressing binder into a film, and then immersing it in the electrolyte at room temperature. The weight of the film was then measured at different times. The DC conductivity was measured on a Solartron Analytical 1400 Cell Test System, where PFPQ-COONa films pasted with Ag were mounted between the two copper electrodes and a constant potential of 3 V was applied.

Electrochemical Measurements. All working electrodes based on conductive binders were prepared by slurry casting method. First, a 2.5 wt % aqueous solution of PFPQ-COONa was prepared. Si nanopowder (Aladdin) was then added into the solution so that the weight ratio of Si and binder was 2:1, followed by stirring at room temperature for 24 h. The slurry was casted onto a Cu foil and dried at room temperature, then it was cut into electrode disks and dried at 135 °C under vacuum over 10 h. The average areal loading of Si on each electrode was approximately 1.2 mg cm^{-2}. The electrochemical measurements were characterized through 2032-type coin half cells with Li metal foil as the negative electrode. $LiPF_6$ (1.2 M) in ethylene carbonate (EC) and diethylene carbonate (DEC) (1:1 v/v) with 30 wt % fluoroethylene carbonate (FEC) was used as the electrolyte. All cells were assembled in an Ar-filled glovebox.

The galvanostatic cycling tests were performed within the voltage range of 0.01 to 1 V (vs Li/Li$^+$) on a Neware battery test system (Newell, China). CV measurements were measured on an electrochemical workstation (CHI 604E) at a scan rate of 0.1 mV s^{-1} in the voltage range of 0.01−3 V (vs Li/Li$^+$). EIS experiments were performed on an electrochemical workstation (CHI 604E). The frequency range applied was from 1 M Hz to 10 Hz.

Calculation Details. The molecular orbitals of polymer segment were calculated with Gaussian09 package. A B3LYP functional was adopted, and the 6-31+G is set as Gaussian basis with diffuse functions both for geometry optimization and self-consistent field calculation.[32,33]

ASSOCIATED CONTENT

Supporting Information

The Supporting Information is available free of charge on the ACS Publications website at DOI: 10.1021/acsami.8b08843.

Representative work for Si electrodes using different conductive binders in recent years (PDF)

AUTHOR INFORMATION

Corresponding Author

*E-mail: panfeng@pkusz.edu.cn.

ORCID

Feng Pan: 0000-0002-8216-1339

Author Contributions

#Authors Y.Z. and L.Y. contributed equally to this work.

Notes

The authors declare no competing financial interest.

ACKNOWLEDGMENTS

The research was financially supported by National Materials Genome Project (2016YFB0700600), Guangdong Innovation Team Project (2013N080) and Shenzhen Science and Technology Research Grant (peacock plan KYPT20141016105435850, JCYJ20151015162256516, JCYJ20150729111733470).

DOI: 10.1021/acsami.8b08843
ACS Appl. Mater. Interfaces 2018, 10, 27795−27800

REFERENCES

(1) Goodenough, J. B.; Kim, Y. Challenges for Rechargeable Li Batteries. *Chem. Mater.* **2010**, *22*, 587−603.

(2) Lu, J.; Chen, Z.; Ma, Z. The Role of Nanotechnology in the Development of Battery Materials for Electric Vehicles. *Nat. Nanotechnol.* **2016**, *11*, 1031−1038.

(3) Li, J.; Dahn, J. R. An In Situ X-Ray Diffraction Study of the Reaction of Li with Crystalline Si. *J. Electrochem. Soc.* **2007**, *154*, A156.

(4) Ryu, J. H.; Kim, J. W.; Sung, Y.-E.; Oh, S. M. Failure Modes of Silicon Powder Negative Electrode in Lithium Secondary Batteries. *Electrochem. Solid-State Lett.* **2004**, *7*, A306.

(5) Chan, C. K.; Peng, H.; Liu, G.; McIlwrath, K.; Zhang, X. F.; Huggins, R. A.; Cui, Y. High-Performance Lithium Battery Anodes Using Silicon Nanowires. *Nat. Nanotechnol.* **2008**, *3*, 31−35.

(6) Liu, N.; Lu, Z.; Zhao, J.; Mcdowell, M. T.; Lee, H. W.; Zhao, W.; Cui, Y. A Pomegranate-Inspired Nanoscale Design for Large-Volume-Change Lithium Battery Anodes. *Nat. Nanotechnol.* **2014**, *9*, 187−192.

(7) Holzapfel, M.; Buqa, H.; Scheifele, W.; Novák, P.; Petrat, F.-M. A New Type of Nano-Sized Silicon/carbon Composite Electrode for Reversible Lithium Insertion. *Chem. Commun.* **2005**, *12*, 1566−1568.

(8) Wang, W.; Kumta, P. N. Nanostructured Hybrid Silicon/Carbon. *ACS Nano* **2010**, *4*, 2233−2241.

(9) Agyeman, D. A.; Song, K.; Lee, G. H.; Park, M.; Kang, Y. M. Carbon-Coated Si Nanoparticles Anchored between Reduced Graphene Oxides as an Extremely Reversible Anode Material for High Energy-Density Li-Ion Battery. *Adv. Energy Mater.* **2016**, *6*, 1−10.

(10) Zhang, Z.; Wang, Y.; Ren, W.; Tan, Q.; Chen, Y.; Li, H.; Zhong, Z.; Su, F. Scalable Synthesis of Interconnected Porous Silicon/carbon Composites by the Rochow Reaction as High-Performance Anodes of Lithium Ion Batteries. *Angew. Chem., Int. Ed.* **2014**, *53*, 5165−5169.

(11) Li, J.-T.; Wu, Z.-Y.; Lu, Y.-Q.; Zhou, Y.; Huang, Q.-S.; Huang, L.; Sun, S.-G. Water Soluble Binder, an Electrochemical Performance Booster for Electrode Materials with High Energy Density. *Adv. Energy Mater.* **2017**, *7*, 1701185.

(12) Magasinski, A.; Zdyrko, B.; Kovalenko, I.; Hertzberg, B.; Burtovyy, R.; Huebner, C. F.; Fuller, T. F.; Luzinov, I.; Yushin, G. Toward Efficient Binders for Li-Ion Battery Si-Based Anodes: Polyacrylic Acid. *ACS Appl. Mater. Interfaces* **2010**, *2*, 3004−3010.

(13) Yue, L.; Zhang, L.; Zhong, H. Carboxymethyl Chitosan: A New Water Soluble Binder for Si Anode of Li-Ion Batteries. *J. Power Sources* **2014**, *247*, 327−331.

(14) Komaba, S.; Yabuuchi, N.; Ozeki, T.; Han, Z. J.; Shimomura, K.; Yui, H.; Katayama, Y.; Miura, T. Comparative Study of Sodium Polyacrylate and Poly(vinylidene Fluoride) as Binders for High Capacity Si-Graphite Composite Negative Electrodes in Li-Ion Batteries. *J. Phys. Chem. C* **2012**, *116*, 1380−1389.

(15) Kovalenko, I.; Zdyrko, B.; Magasinski, A.; Hertzberg, B.; Milicev, Z.; Burtovyy, R.; Luzinov, I.; Yushin, G. A Major Constituent of Brown Algae for Use in High-Capacity Li-Ion Batteries. *Science (Washington, DC, U. S.)* **2011**, *334*, 75−79.

(16) Ryou, M. H.; Kim, J.; Lee, I.; Kim, S.; Jeong, Y. K.; Hong, S.; Ryu, J. H.; Kim, T. S.; Park, J. K.; Lee, H.; Choi, J. W. Mussel-Inspired Adhesive Binders for High-Performance Silicon Nanoparticle Anodes in Lithium-Ion Batteries. *Adv. Mater.* **2013**, *25*, 1571−1576.

(17) Liu, Y.; Matsumura, T.; Imanishi, N.; Hirano, A.; Ichikawa, T.; Takeda, Y. Preparation and Characterization of Si/C Composite Coated with Polyaniline as Novel Anodes for Li-Ion Batteries. *Electrochem. Solid-State Lett.* **2005**, *8*, A599.

(18) Wu, H.; Yu, G.; Pan, L.; Liu, N.; McDowell, M. T.; Bao, Z.; Cui, Y. Stable Li-Ion Battery Anodes by in-Situ Polymerization of Conducting Hydrogel to Conformally Coat Silicon Nanoparticles. *Nat. Commun.* **2013**, *4*, 1943−1946.

(19) Shao, D.; Zhong, H.; Zhang, L. Water-Soluble Conductive Composite Binder Containing PEDOT: PSS as Conduction Promoting Agent for Si Anode of Lithium-Ion Batteries. *ChemElectroChem* **2014**, *1*, 1679−1687.

(20) Wang, L.; Liu, T.; Peng, X.; Zeng, W.; Jin, Z.; Tian, W.; Gao, B.; Zhou, Y.; Chu, P. K.; Huo, K. Highly Stretchable Conductive Glue for High-Performance Silicon Anodes in Advanced Lithium-Ion Batteries. *Adv. Funct. Mater.* **2018**, *28*, 1−8.

(21) Higgins, T. M.; Park, S. H.; King, P. J.; Zhang, C.; McEvoy, N.; Berner, N. C.; Daly, D.; Shmeliov, A.; Khan, U.; Duesberg, G.; Nicolosi, V.; Coleman, J. N. A Commercial Conducting Polymer as Both Binder and Conductive Additive for Silicon Nanoparticle-Based Lithium-Ion Battery Negative Electrodes. *ACS Nano* **2016**, *10*, 3702−3713.

(22) Liu, J.; Zhang, Q.; Zhang, T.; Li, J. T.; Huang, L.; Sun, S. G. A Robust Ion-Conductive Biopolymer as a Binder for Si Anodes of Lithium-Ion Batteries. *Adv. Funct. Mater.* **2015**, *25*, 3599−3605.

(23) Liu, G.; Xun, S.; Vukmirovic, N.; Song, X.; Olalde-Velasco, P.; Zheng, H.; Battaglia, V. S.; Wang, L.; Yang, W. Polymers with Tailored Electronic Structure for High Capacity Lithium Battery Electrodes. *Adv. Mater.* **2011**, *23*, 4679−4683.

(24) Zhao, H.; Lu, P.; Jiang, M.; Song, X.; Zheng, Z.; Zhou, X.; Fu, Y.; Xiao, X.; Liu, Z.; Battaglia, V. S.; Zaghib, K.; Liu, G.; Wang, Z.; Shi, F.; Adelbast, G. Toward Practical Application of Functional Conductive Polymer Binder for a High-Energy Lithium-Ion Battery Design Toward Practical Application of Functional Conductive Polymer Binder for a High-Energy Lithium-Ion Battery Design. *Nano Lett.* **2014**, *14*, 6704−6710.

(25) Wu, M.; Xiao, X.; Vukmirovic, N.; Xun, S.; Das, P. K.; Song, X.; Olalde-Velasco, P.; Wang, D.; Weber, A. Z.; Wang, L. W.; Battaglia, V. S.; Yang, W.; Liu, G. Toward an Ideal Polymer Binder Design for High-Capacity Battery Anodes. *J. Am. Chem. Soc.* **2013**, *135*, 12048−12056.

(26) Liu, D.; Zhao, Y.; Tan, R.; Tian, L.-L.; Liu, Y.; Chen, H.; Pan, F. Novel Conductive Binder for High-Performance Silicon Anodes in Lithium Ion Batteries. *Nano Energy* **2017**, *36*, 206−212.

(27) Kim, S.-M.; Kim, M. H.; Choi, S. Y.; Lee, J. G.; Jang, J.; Lee, J. B.; Ryu, J. H.; Hwang, S. S.; Park, J.-H.; Shin, K.; Kim, Y. G.; Oh, S. M. Poly(phenanthrenequinone) as a Conductive Binder for Nano-Sized Silicon Negative Electrodes. *Energy Environ. Sci.* **2015**, *8*, 1538−1543.

(28) Mazouzi, D.; Lestriez, B.; Roué, L.; Guyomard, D. Silicon Composite Electrode with High Capacity and Long Cycle Life. *Electrochem. Solid-State Lett.* **2009**, *12*, A215−A218.

(29) Koo, B.; Kim, H.; Cho, Y.; Lee, K. T.; Choi, N. S.; Cho, J. A Highly Cross-Linked Polymeric Binder for High-Performance Silicon Negative Electrodes in Lithium Ion Batteries. *Angew. Chem., Int. Ed.* **2012**, *51*, 8762−8767.

(30) Shimizu, A.; Kuramoto, H.; Tsujii, Y.; Nokami, T.; Inatomi, Y.; Hojo, N.; Suzuki, H.; Yoshida, J. I. Introduction of Two Lithiooxycarbonyl Groups Enhances Cyclability of Lithium Batteries with Organic Cathode Materials. *J. Power Sources* **2014**, *260*, 211−217.

(31) Jaffe, A.; Saldivar Valdes, A.; Karunadasa, H. I. Quinone-Functionalized Carbon Black Cathodes for Lithium Batteries with High Power Densities. *Chem. Mater.* **2015**, *27*, 3568−3571.

(32) Hehre, W. J.; Ditchfield, K.; Pople, J. A. Self-Consistent Molecular Orbital Methods. XII. Further Extensions of Gaussian-Type Basis Sets for Use in Molecular Orbital Studies of Organic Molecules. *J. Chem. Phys.* **1972**, *56*, 2257−2261.

(33) Francl, M. M.; Pietro, W. J.; Hehre, W. J.; Binkley, J. S.; Gordon, M. S.; DeFrees, D. J.; Pople, J. A. Self-Consistent Molecular Orbital Methods. XXIII. A Polarization-Type Basis Set for Second-Row Elements. *J. Chem. Phys.* **1982**, *77*, 3654−3665.

DOI: 10.1021/acsami.8b08843
ACS Appl. Mater. Interfaces 2018, 10, 27795−27800